Brazilian Journal
of Chemical
Engineering

ISSN 0104-6632
Printed in Brazil
www.abeq.org.br/bjche

Vol. 30, No. 04, pp. 883 - 896, October - December, 2013

INTEGRAL TRANSFORM SOLUTION OF NATURAL CONVECTION IN A SQUARE CAVITY WITH VOLUMETRIC HEAT GENERATION

C. An[1,2], C. B. Vieira[1] and J. Su[1*]

[1]Nuclear Engineering Program, COPPE, Phone: + (55) (21) 2562 8448, Fax: + (55) (21) 2562 8444,
Universidade Federal do Rio de Janeiro, CP 68509, CEP: 21941-972, Rio de Janeiro - RJ, Brazil.
E-mail: sujian@nuclear.ufrj.br
[2]Offshore Oil/Gas Research Center, College of Mechanical and Transportation Engineering,
China University of Petroleum (Beijing), Beijing 102249, China.

(Submitted: January 4, 2012 ; Revised: October 9, 2012 ; Accepted: October 10, 2012)

Abstract - The generalized integral transform technique (GITT) is employed to obtain a hybrid numerical-analytical solution of natural convection in a cavity with volumetric heat generation. The hybrid nature of this approach allows for the establishment of benchmark results in the solution of non-linear partial differential equation systems, including the coupled set of heat and fluid flow equations that govern the steady natural convection problem under consideration. Through performing the GITT, the resulting transformed ODE system is then numerically solved by making use of the subroutine DBVPFD from the IMSL Library. Therefore, numerical results under user prescribed accuracy are obtained for different values of Rayleigh numbers, and the convergence behavior of the proposed eigenfunction expansions is illustrated. Critical comparisons against solutions produced by ANSYS CFX 12.0 are then conducted, which demonstrate excellent agreement. Several sets of reference results for natural convection with volumetric heat generation in a bi-dimensional square cavity are also provided for future verification of numerical results obtained by other researchers.
Keywords: Natural convection; Square cavity; Volumetric heat generation; Integral transform; Hybrid solution.

INTRODUCTION

The investigations of natural convection flow and heat transfer processes, driven by buoyancy forces due to density differences caused by temperature variations in the fluid, have been motivated by their importance in many natural and industrial problems (Cheng, 2006, 2010; Kairi and Murthy, 2011). In all these investigations, considerable work has been done on the study of natural convection in volumetrically heated cavities due to applications in various technological areas such as nuclear reactor design (Baker *et al*., 1976a,b; Qiu *et al*., 2010), geophysics (Runcorn, 1962; Mckenzie *et al*., 1974) and astrophysics (Bethe, 1968; Tritton, 1975).

Many experimental, analytical and numerical approaches have been employed to investigate the characteristics of flow and heat transfer in enclosures with volumetric heat generation. Lee and Goldstein (1988) used a Mach-Zehnder interferometer to investigate experimentally the temperature distribution and the heat transfer rates within an inclined square enclosure containing fluid with internal energy sources bounded by four rigid planes of constant equal temperature. The experimental results of Lee and Goldstein (1988) were later employed to compare with the numerical solutions obtained by May (1991). Based on a finite-difference procedure, Acharya and Goldstein (1985) and Rahman and Sharif (2003) separately studied natural convection

*To whom correspondence should be addressed

in an inclined and vertical square enclosure containing internal energy sources and subjected to external heating, and analyzed the flow patterns for different Rayleigh numbers (both internal and external). To verify the steady-state experimental observations of Kawara *et al*. (1990), Fusegi *et al*. (1992) solved numerically natural convection in a differentially heated rectangular cavity with internal heat generation by a control volume-based finite difference technique. Using a finite-volume technique, Di Piazza and Ciofalo (2000) performed direct numerical two-dimensional simulations of low-Prandtl number free convection in a volumetrically heated rectangular enclosure with aspect ratio $(AR = 4)$, adiabatic top/bottom walls and isothermal side walls. Different flow regimes (steady-state, periodic and chaotic) were obtained based on the values of the Grashof number. Extending previous work, Arcidiacono *et al*. (2001) and Arcidiacono and Ciofalo (2001) predicted the flow and temperature fields at different Grashof numbers in a square cavity $(AR = 1)$, and subsequently in a shallow cavity $(AR = 0.25)$. By expressing the governing equations in terms of streamfunction, vorticity and temperature formulation, Joshi *et al*. (2006) conducted a semi-analytical study of natural convection in cavities of different aspect ratios with uniform volumetric heat generation, considering two different boundary conditions, viz., all isothermal walls and only adiabatic horizontal walls. Daniels and Jones (1998) used matched asymptotic expansions method to analyze natural convection in a shallow rectangular cavity due to internal heat generation, where the nonlinear convective effects were studied. Moreover, Qiu *et al*. (2010) investigated numerically the local Nusselt number, the flow and temperature field at different conditions of two-dimensional natural convection with non-uniform heat generation in a confined enclosure.

Recently, An and Su (2011) employed a hybrid numerical-analytical approach, known as GITT, to study the dynamic response of clamped axially moving beams, where excellent convergence behavior of the integral transform solution was shown by comparing the vibration displacement of different points along the beam length. Indeed, past studies have shown that GITT is a powerful and applicable method for solving diffusion and convection-diffusion problems in heat and fluid flow (Cotta, 1993; Cotta and Mikhailov, 1997; Cotta, 1998). The most interesting feature of this technique is the automatic and straightforward global error control procedure, which makes it particularly suitable for benchmarking purposes, and the only mild increase in overall computational effort with increasing number of independent variables. Leal *et al*. (1999) examined the convergence characteristics of the GITT solution for the steady laminar natural convection of a Newtonian fluid inside rectangular enclosures differentially heated at the vertical walls and demonstrated the usefulness of this integral transform method by performing critical comparisons against previously reported benchmark solutions. As a continuation of their research, Leal *et al*. (2000) studied the behavior of fluid flow and heat transfer for transient laminar natural convection with variable physical properties inside cavities, and presented the advantages of utilizing the false transient technique for obtaining steady solutions with the GITT method.

The objective of this work is to extend the GITT method to study natural convection in a square cavity with uniform volumetric heat generation, which is one of the key issues concerned in nuclear safety. Since there is no approximation involved in the analytical derivation of the GITT approach, and the problem solution is represented by the sum of a rapidly-converging in finite series, the GITT solutions with the desired precision may serve as benchmarks for testing other numerical methods. Two different boundary conditions are analyzed for the cavity: (a) horizontal walls adiabatic and vertical walls isothermal, (b) all walls isothermal. In the next section, the mathematical formulation of the problem of natural convection in a volumetrically heated cavity is presented. Then, the hybrid numerical-analytical solution is obtained by carrying out integral transform, and numerical results with automatic global accuracy control are presented for different boundary conditions. A comparison against the simulation results of square cavities obtained by ANSYS CFX 12.0 is then performed to assess the accuracy and convergence of the present approach.

MATHEMATICAL FORMULATION

Consider a square cavity of side H, containing a fluid with uniform volumetric heat generation rate q'''. Two different boundary conditions are considered in the present study: (a) the horizontal walls are adiabatic and the vertical walls are isothermal, maintained at a constant temperature T_0, and (b) all walls are isothermal, maintained at a contant temperature T_0, as illustrated in Fig. 1.

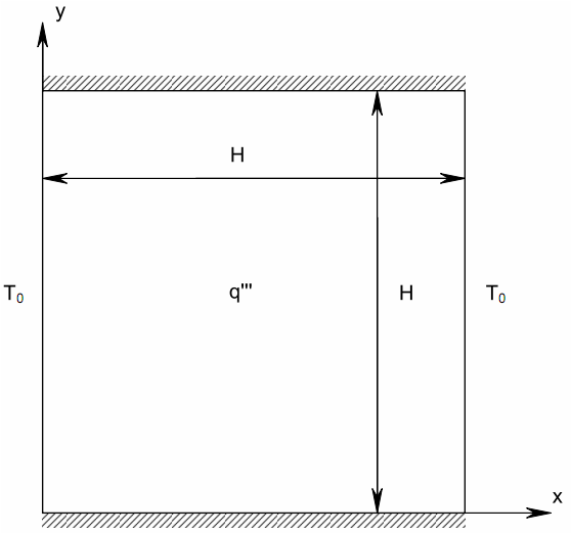

(a)

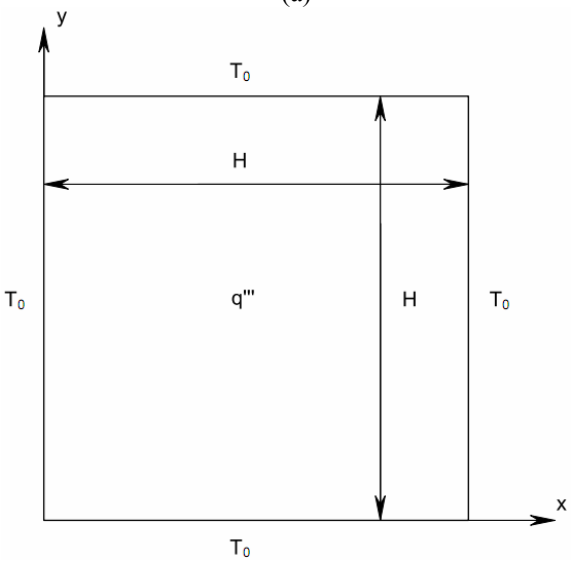

(b)

Figure 1: Schematic of the square cavity with volumetric heat generation: (a) horizontal walls are adiabatic and vertical walls are isothermal, (b) all walls are isothermal.

The governing equations for two-dimensional steady-state natural convection, under the Boussinesq approximation, are written as:

$$\frac{\partial u}{\partial x}+\frac{\partial v}{\partial y}=0, \tag{1}$$

$$\rho\left(u\frac{\partial u}{\partial x}+v\frac{\partial u}{\partial y}\right)=-\frac{\partial p}{\partial x}+\mu\left(\frac{\partial^2 u}{\partial x^2}+\frac{\partial^2 u}{\partial y^2}\right), \tag{2a}$$

$$\rho\left(u\frac{\partial v}{\partial x}+v\frac{\partial v}{\partial y}\right)=-\frac{\partial p}{\partial y}+\mu\left(\frac{\partial^2 v}{\partial x^2}+\frac{\partial^2 v}{\partial y^2}\right)+\rho\beta\left(T-T_0\right)g, \tag{2b}$$

$$\rho c_p\left(u\frac{\partial T}{\partial x}+v\frac{\partial T}{\partial y}\right)=k\left(\frac{\partial^2 T}{\partial x^2}+\frac{\partial^2 T}{\partial y^2}\right)+q''', \tag{3}$$

where x and y are respectively the horizontal and vertical spatial coordinates, u and v the velocity components, p the pressure, T the temperature, g the gravitational acceleration, ρ the density, β the thermal expansion coefficient, c_p the specific heat, and k the thermal conductivity of the fluid.

The boundary conditions for the two problems considered are respectively given by:

$$u=v=0,\ T=T_0 \quad \text{at } x=0, \tag{4a}$$

$$u=v=0,\ T=T_0 \quad \text{at } x=H, \tag{4b}$$

$$u=v=0,\ \frac{\partial T}{\partial y}=0 \quad \text{at } y=0, \tag{4c}$$

$$u=v=0,\ \frac{\partial T}{\partial y}=0 \quad \text{at } y=H \tag{4d}$$

and

$$u=v=0,\ T=T_0 \quad \text{at } x=0, \tag{5a}$$

$$u=v=0,\ T=T_0 \quad \text{at } x=H, \tag{5b}$$

$$u=v=0,\ T=T_0 \quad \text{at } y=0, \tag{5c}$$

$$u=v=0,\ T=T_0 \quad \text{at } y=H. \tag{5d}$$

For two-dimensional incompressible flow, the stream-function ψ^* can be defined, which satisfies identically the continuity equation:

$$u=\frac{\partial \psi^*}{\partial y},\ v=-\frac{\partial \psi^*}{\partial x}. \tag{6a,b}$$

The governing Equations (2a), (2b), (3) can be combined into the stream-function only formulation as follows:

$$\frac{\partial \psi^*}{\partial y}\frac{\partial \nabla^2 \psi^*}{\partial x} - \frac{\partial \psi^*}{\partial x}\frac{\partial \nabla^2 \psi^*}{\partial y} = \nu \nabla^4 \psi^* - \beta g \frac{\partial T}{\partial x}, \quad (7)$$

$$\frac{\partial \psi^*}{\partial y}\frac{\partial T}{\partial x} - \frac{\partial \psi^*}{\partial x}\frac{\partial T}{\partial y} = \alpha \nabla^2 T + \frac{q'''}{\rho c_p}, \quad (8)$$

with the following boundary conditions:

$$\psi^* = \frac{\partial \psi^*}{\partial x} = 0, \ T = T_0 \quad \text{at } x = 0, \quad (9a)$$

$$\psi^* = \frac{\partial \psi^*}{\partial x} = 0, \ T = T_0 \quad \text{at } x = H, \quad (9b)$$

$$\psi^* = \frac{\partial \psi^*}{\partial y} = 0, \ \frac{\partial T}{\partial y} = 0 \quad \text{at } y = 0, \quad (9c)$$

$$\psi^* = \frac{\partial \psi^*}{\partial y} = 0, \ \frac{\partial T}{\partial y} = 0 \quad \text{at } y = H \quad (9d)$$

and

$$\psi^* = \frac{\partial \psi^*}{\partial x} = 0, \ T = T_0 \quad \text{at } x = 0, \quad (10a)$$

$$\psi^* = \frac{\partial \psi^*}{\partial x} = 0, \ T = T_0 \quad \text{at } x = H, \quad (10b)$$

$$\psi^* = \frac{\partial \psi^*}{\partial y} = 0, \ T = T_0 \quad \text{at } y = 0, \quad (10c)$$

$$\psi^* = \frac{\partial \psi^*}{\partial y} = 0, \ T = T_0 \quad \text{at } y = H. \quad (10d)$$

Dimensionless variables can be introduced as follows:

$$x = \frac{x^*}{H}, \ y = \frac{y^*}{H}, \ U = \frac{u}{\alpha / H}, \ V = \frac{v}{\alpha / H},$$

$$\psi = \frac{\psi^*}{\alpha}, \ \theta = \frac{T - T_0}{q''' H^2 / k}, \ Pr = \frac{\nu}{\alpha} = \frac{\mu c_p}{k}, \quad (11)$$

$$Ra = \frac{\beta g q''' H^5}{\alpha \nu k},$$

where x^* and y^* identify the dimensional spatial variables, ν the kinematic viscosity and α the thermal diffusivity. The dimensionless governing Equations (7), (8) are written as follows:

$$\frac{\partial \psi}{\partial y}\frac{\partial \nabla^2 \psi}{\partial x} - \frac{\partial \psi}{\partial x}\frac{\partial \nabla^2 \psi}{\partial y} = Pr \nabla^4 \psi - PrRa \frac{\partial \theta}{\partial x}, \quad (12)$$

$$\frac{\partial \psi}{\partial y}\frac{\partial \theta}{\partial x} - \frac{\partial \psi}{\partial x}\frac{\partial \theta}{\partial y} = \nabla^2 \theta + 1, \quad (13)$$

which can be further expressed by

$$\frac{\partial^4 \psi}{\partial y^4} + 2\frac{\partial^4 \psi}{\partial x^2 y^2} + \frac{\partial^4 \psi}{\partial x^4} = \frac{1}{Pr}\left[\frac{\partial \psi}{\partial y}\frac{\partial^3 \psi}{\partial x^3} + \frac{\partial \psi}{\partial y}\frac{\partial^3 \psi}{\partial y^2 \partial x} - \frac{\partial \psi}{\partial x}\frac{\partial^3 \psi}{\partial x^2 y} - \frac{\partial \psi}{\partial x}\frac{\partial^3 \psi}{\partial y^3}\right] + Ra\frac{\partial \theta}{\partial x}, \quad (14)$$

$$\frac{\partial^2 \theta}{\partial y^2} + \frac{\partial^2 \theta}{\partial x^2} = \frac{\partial \psi}{\partial y}\frac{\partial \theta}{\partial x} - \frac{\partial \psi}{\partial x}\frac{\partial \theta}{\partial y} - 1 \quad (15)$$

with the following boundary conditions:

$$\psi = \frac{\partial \psi}{\partial x} = 0, \ \psi = 0 \quad \text{at } x = 0, \quad (16a)$$

$$\psi = \frac{\partial \psi}{\partial x} = 0, \ \theta = 0 \quad \text{at } x = 0, \quad (16b)$$

$$\psi = \frac{\partial \psi}{\partial y} = 0, \ \frac{\partial \theta}{\partial y} = 0 \quad \text{at } y = 0, \quad (16c)$$

$$\psi = \frac{\partial \psi}{\partial y} = 0, \ \frac{\partial \theta}{\partial y} = 0 \quad \text{at } y = 1 \quad (16d)$$

and

$$\psi = \frac{\partial \psi}{\partial x} = 0, \ \theta = 0 \quad \text{at } x = 0, \quad (17a)$$

$$\psi = \frac{\partial \psi}{\partial x} = 0, \ \theta = 0 \quad \text{at } x = 1, \quad (17b)$$

$$\psi = \frac{\partial \psi}{\partial y} = 0, \ \theta = 0 \quad \text{at } y = 0, \quad (17c)$$

$$\psi = \frac{\partial \psi}{\partial y} = 0, \ \theta = 0 \quad \text{at } y = 1, \quad (17d)$$

respectively.

INTEGRAL TRANSFORM SOLUTION

The main procedures of the GITT-type integral transformation process are: (a) to choose auxiliary eigenvalue problems from homogeneous versions of the original problem; (b) to obtain eigenvalues and eigenfunctions which satisfy the orthogonality property; (c) to define the integral transform pair, including the transform formula and the inverse formula; (d) to transform the original problem with transform formula to obtain a set of ordinary differential equations with the calculable coefficients; (e) to solve the ordinary differential equation system by mathematical tools software or codes, such as *Mathematica*, IMSL Library, etc.; and (f) to obtain the original problem solutions using the inverse formula.

According to the principle of the generalized integral transform technique, the auxiliary eigenvalue problem needs to be chosen for the dimensionless governing Equations (14), (15) with the homogenous boundary conditions (16 or 17). The 'x' direction is selected to be eliminated through integral transformation, and the eigenvalue problem of the biharmonic-type, previously studied in Leal *et al*. (1999), is adopted for the streamfunction representation as follows:

$$\frac{\mathrm{d}^4 X_i(x)}{\mathrm{d}x^4} = \mu_i^4 X_i(x), \quad 0 < x < 1, \tag{18a}$$

with the following boundary conditions

$$X_i(0) = 0, \quad \frac{\mathrm{d}X_i(0)}{\mathrm{d}x} = 0, \tag{18b,c}$$

$$X_i(1) = 0, \quad \frac{\mathrm{d}X_i(1)}{\mathrm{d}x} = 0, \tag{18d,e}$$

where $X_i(x)$ and μ_i are, respectively, the eigenfunctions and eigenvalues of problem (18). The eigenfunctions satisfy the following orthogonality property

$$\int_0^1 X_i(x) X_j(x)\,\mathrm{d}x = \delta_{ij} N_i, \tag{19}$$

with $\delta_{ij} = 0$ for $i \neq j$, and $\delta_{ij} = 1$ for $i = j$. The norm, or normalization integral, is written as

$$N_i = \int_0^1 X_i^2(x)\,\mathrm{d}x. \tag{20}$$

The related eigenfunctions of problem (18) are given by:

$$X_i(x) = \begin{cases} \dfrac{\cos[\mu_i(x-1/2)]}{\cos[\mu_i/2]} \\ -\dfrac{\cosh[\mu_i(x-1/2)]}{\cosh[\mu_i/2]}, \text{for } i \text{ odd}, \\ \dfrac{\sin[\mu_i(x-1/2)]}{\sin[\mu_i/2]} \\ -\dfrac{\sinh[\mu_i(x-1/2)]}{\sinh[\mu_i/2]}, \text{for } i \text{ even}, \end{cases} \tag{21a,b}$$

where the eigenvalues are obtained from the transcendental equation:

$$\tanh(\mu_i/2) = \begin{cases} -\tan(\mu_i/2), & \text{for } i \text{ odd}, \\ \tan(\mu_i/2), & \text{for } i \text{ even}, \end{cases} \tag{22a,b}$$

and the normalization integral is evaluated as

$$N_i = 1, \qquad i = 1,2,3,\ldots \tag{23}$$

Therefore, the normalized eigenfunction coincides, in this case, with the original eigenfunction itself, i.e.

$$\tilde{X}_i(x) = \frac{X_i(x)}{N_i^{1/2}}. \tag{24}$$

For the temperature expansion, the classical second-order diffusion operator yields a Sturm-Liouville type problem, readily solved with the appropriate boundary conditions of the first kind at the lateral walls, to yield the eigenfunctions and related quantities:

$$\phi_m(x) = \sin\beta_m x, \qquad m = 1,2,3,\ldots, \tag{25}$$

where the eigenvalues are given by

$$\beta_m = m\pi, \qquad m = 1,2,3,\ldots \tag{26}$$

and the norm evaluation yields

$$M_m = 1/2, \qquad m = 1,2,3,\ldots \tag{27}$$

The normalized eigenfunction $\tilde{\phi}_m$ then becomes

$$\tilde{\phi}_m(x) = \frac{\phi_m(x)}{M_m^{1/2}}. \tag{28}$$

The solution methodology proceeds towards the proposition of the integral transform pair for the potentials, the integral transformation itself and the inversion formula. For the streamfunction field:

$$\psi_i(y) = \int_0^1 \tilde{X}_i(x)\psi(x,y)\mathrm{d}x, \quad \text{transform,} \tag{29a}$$

$$\psi(x,y) = \sum_{i=1}^{\infty} \tilde{X}_i(x)\overline{\psi}_i(y), \quad \text{inverse,} \tag{29b}$$

and for the temperature field:

$$\overline{\theta}_m(y) = \int_0^1 \tilde{\phi}_m(x)\theta(x,y)\mathrm{d}x, \quad \text{transform,} \tag{30a}$$

$$\theta(x,y) = \sum_{i=1}^{\infty} \tilde{\phi}_m(x)\overline{\theta}_m(y), \quad \text{inverse.} \tag{30b}$$

The integral transformation process is now employed through operation of (14) with $\int_0^1 \tilde{X}_i(x)dx$, , to find the transformed streamfunction system:

$$\frac{\mathrm{d}^4\overline{\psi}_i(y)}{\mathrm{d}y^4} = \frac{1}{Pr}\sum_{j=1}^{\infty}\sum_{k=1}^{\infty}\left[A_{ijk}\frac{\mathrm{d}\overline{\psi}_j}{\mathrm{d}y}\overline{\psi}_k + B_{ijk}\frac{\mathrm{d}\overline{\psi}_j}{\mathrm{d}y}\frac{\mathrm{d}^2\overline{\psi}_k}{\mathrm{d}y^2} \right.$$

$$\left. -C_{ijk}\overline{\psi}_j\frac{\mathrm{d}\overline{\psi}_k}{\mathrm{d}y} - B_{ijk}\frac{\mathrm{d}^3\overline{\psi}_j}{\mathrm{d}y^3}\overline{\psi}_k \right] - \mu_i^4\overline{\psi}_i \tag{31}$$

$$-2\sum_{j=1}^{\infty}D_{ij}\frac{\mathrm{d}^2\overline{\psi}_j}{\mathrm{d}y^2} + Ra\sum_{m=1}^{\infty}E_{im}\overline{\theta}_m, \; i = 1,2,3,\ldots,$$

where the related coefficients are obtained analytically through symbolic computation packages, such as *Mathematica* (Wolfram, 2003), and automatically generated in Fortran form through their definitions:

$$A_{ijk} = \int_0^1 \tilde{X}_i\tilde{X}_j\tilde{X}_k'''\mathrm{d}x, \; B_{ijk} = \int_0^1 \tilde{X}_i\tilde{X}_j\tilde{X}_k'\mathrm{d}x, \tag{32a,b}$$

$$C_{ijk} = \int_0^1 \tilde{X}_i\tilde{X}_j'\tilde{X}_k''\mathrm{d}x, \; D_{ij} = \int_0^1 \tilde{X}_i\tilde{X}_j''\mathrm{d}x, \tag{32c,d}$$

$$E_{im} = \int_0^1 \tilde{X}_i\tilde{\phi}_m'\mathrm{d}x, \tag{32e}$$

Similarly, Eq. (15) is operated on with $\int_0^1 \tilde{\phi}_m(x)\mathrm{d}x$, to yield the transformed temperature problem:

$$\frac{\mathrm{d}^2\overline{\theta}_m(y)}{\mathrm{d}y^2} = \sum_{n=1}^{\infty}\sum_{j=1}^{\infty}\left[Q_{mnj}\overline{\theta}_n\frac{\mathrm{d}\overline{\psi}_j}{\mathrm{d}y} - S_{mnj}\frac{\mathrm{d}\overline{\theta}_n}{\mathrm{d}y}\overline{\psi}_j \right] + \beta_m^2\overline{\theta}_m - P_m, \; m = 1,2,3,\ldots, \tag{33}$$

where the associated coefficients, symbolically computed and automatically generated within the code, are obtained from

$$Q_{mnj} = \int_0^1 \tilde{\phi}_m\tilde{\phi}_n'\tilde{X}_j\mathrm{d}x, \tag{34a}$$

$$S_{mnj} = \int_0^1 \tilde{\phi}_m\tilde{\phi}_n\tilde{X}_j'\mathrm{d}x, \quad P_m = \int_0^1 \tilde{\phi}_m\mathrm{d}x. \tag{34b,c}$$

The resulting coupled infinite system of ordinary differential equations with boundary condition at two points for the transformed potentials is then described by Equations (31) and (33), together with the integral transformed boundary conditions:

$$\overline{\psi}_i(0) = 0, \; \frac{\mathrm{d}\overline{\psi}_i(0)}{\mathrm{d}y} = 0, \; \frac{\mathrm{d}\overline{\theta}_m(0)}{\mathrm{d}y} = 0, \tag{35a,b,c}$$

$$\overline{\psi}_i(1) = 0, \; \frac{\mathrm{d}\overline{\psi}_i(1)}{\mathrm{d}y} = 0, \; \frac{\mathrm{d}\overline{\theta}_m(1)}{\mathrm{d}y} = 0, \tag{35d,e,f}$$

and

$$\overline{\psi}_i(0) = 0, \; \frac{\mathrm{d}\overline{\psi}_i(0)}{\mathrm{d}y} = 0, \; \overline{\theta}_m(0) = 0, \tag{36a,b,c}$$

$$\overline{\psi}_i(1) = 0, \; \frac{\mathrm{d}\overline{\psi}_i(1)}{\mathrm{d}y} = 0, \; \overline{\theta}_m(1) = 0, \tag{36d,e,f}$$

respectively.

For computational purposes, the expansions are truncated at sufficiently large orders, NV and NT, respectively. This truncated system is then solved by a computer program developed in Fortran 90, based on the use of the subroutine DBVPFD from the IMSL Library (IMSL, 2003) with automatic control of the local relative error (10^{-4} is selected for this problem). For this purpose, the system composed of (31) and (33) is first rewritten as a first order ODE system, i.e.

$$\boldsymbol{w}' = f\left(\boldsymbol{w}, \mathrm{y}\right) \tag{37}$$

where the solution vector, w, is defined as

$$w = \left\{ \overline{\psi}_1, \frac{\mathrm{d}\overline{\psi}_1}{\mathrm{d}y}, \frac{\mathrm{d}^2\overline{\psi}_1}{\mathrm{d}y^2}, \frac{\mathrm{d}^3\overline{\psi}_1}{\mathrm{d}y^3}, \ldots, \overline{\psi}_{NV}, \frac{\mathrm{d}\overline{\psi}_{NV}}{\mathrm{d}y}, \right.$$
$$\left. \frac{\mathrm{d}^2\overline{\psi}_{NV}}{\mathrm{d}y^2}, \frac{\mathrm{d}^3\overline{\psi}_{NV}}{\mathrm{d}y^3}, \overline{\theta}_1, \frac{\mathrm{d}\overline{\theta}_1}{\mathrm{d}y}, \ldots, \overline{\theta}_{NT}, \frac{\mathrm{d}\overline{\theta}_{NT}}{\mathrm{d}y} \right\}^{\mathrm{T}} \tag{38}$$

Once the transformed potentials, $\overline{\psi}_i$ and $\overline{\theta}_m$, have been numerically evaluated under controlled accuracy, the inversion formulae (29b) and (30b) are recalled to provide explicit analytical expressions, in the 'y' direction, for the original potentials $\psi(x,y)$ and $\theta(x,y)$. The velocity components, $U(x,y)$ and $V(x,y)$, are analytically expressed from the inversion formula (29b) and the streamfunction definition, in the form:

$$U = \sum_{i=1}^{NV} \tilde{X}_i(x) \frac{\mathrm{d}\overline{\psi}_i(y)}{\mathrm{d}y}, \quad V = -\sum_{i=1}^{NV} \frac{\mathrm{d}\tilde{X}_i(x)}{\mathrm{d}x} \overline{\psi}_i(y). \tag{39a,b}$$

RESULTS AND DISCUSSION

We now present numerical results for natural convection in a cavity with volumetric heat generation. Two different boundary conditions are considered: i) adiabatic horizontal walls and isothermal vertical walls, ii) all walls isothermal. A Prandtl number of 0.7 is employed in this study. The solutions of the systems (31, 33) are obtained with $NV \le 40$ and $NT \le 40$ to analyze the convergence behavior, then the accuracy is verified by the numerical results obtained with ANSYS CFX 12.0, where a 200×200 computational grid is used.

The streamline and isotherm contour plots for an internally heated square enclosure with adiabatic horizontal walls and isothermal vertical walls at $Ra = 10000$ are illustrated in Fig. 2. The flow field takes on a pattern possessing bilateral symmetry, where two counter-rotating convective rolls appear. The dimensionless temperature is maximum at the top of the vertical centerline and decreases near the vertical walls, which explains why the flows rise in the central region of the cavity, divide close to the top adiabatic wall, then move downward separately along the vertical walls.

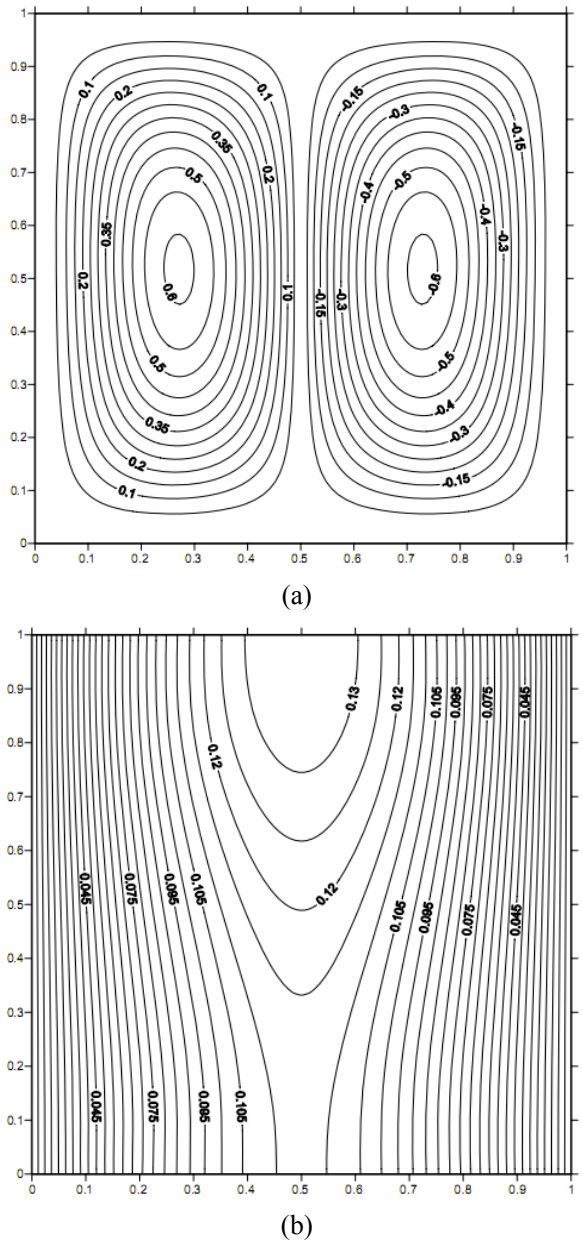

Figure 2: Contour plots for an internally heated square enclosure with adiabatic horizontal walls and isothermal vertical walls at $Ra = 10000$: (a) streamline, (b) isotherm.

The convergence behavior of the GITT solution is examined by computing the dimensionless temperature θ and dimensionless vertical velocity V with different truncation orders NV and NT at the positions $(0.5,0.0)$, $(0.5,0.5)$ and $(0.5,1.0)$, , as presented in Table 1. For the dimensionless temperature, it can be observed that convergence is essentially achieved with reasonably low truncation orders ($NV \le 20$ and $NT \le 20$).

Table 1: Convergence of the dimensionless temperature θ and dimensionless vertical velocity V with different truncation orders NV and NT for the cavity with adiabatic horizontal walls, and comparison with the numerical solution by ANSYS CFX 12.0 at different positions

	$Ra = 1000$	$Ra = 2500$	$Ra = 4900$	$Ra = 7500$	$Ra = 10000$
θ(0.5, 0.0)					
$NV = 10$, $NT = 10$	0.123705	0.121610	0.118193	0.114540	0.111186
$NV = 20$, $NT = 20$	0.123635	0.121540	0.118123	0.114470	0.111115
$NV = 30$, $NT = 30$	0.123646	0.121551	0.118134	0.114480	0.111126
$NV = 40$, $NT = 40$	0.123642	0.121547	0.118130	0.114477	0.111122
ANSYS CFX 12.0	0.123658	0.121555	0.118133	0.114473	0.111113
θ(0.5, 0.5)					
$NV = 10$, $NT = 10$	0.125006	0.124720	0.123798	0.122272	0.120450
$NV = 20$, $NT = 20$	0.124937	0.124652	0.123729	0.122204	0.120382
$NV = 30$, $NT = 30$	0.124947	0.124662	0.123739	0.122214	0.120392
$NV = 40$, $NT = 40$	0.124944	0.124658	0.123736	0.122211	0.120389
ANSYS CFX 12.0	0.124956	0.124671	0.123745	0.122216	0.120390
θ(0.5, 1.0)					
$NV = 10$, $NT = 10$	0.126372	0.128232	0.130875	0.133204	0.134903
$NV = 20$, $NT = 20$	0.126304	0.128164	0.130807	0.133138	0.134837
$NV = 30$, $NT = 30$	0.126314	0.128174	0.130818	0.133148	0.134848
$NV = 40$, $NT = 40$	0.126311	0.128171	0.130814	0.133145	0.134844
ANSYS CFX 12.0	0.126350	0.128189	0.130835	0.133168	0.134867
V(0.5, 0.5)					
$NV = 10$, $NT = 10$	0.438831	1.093457	2.120198	3.186796	4.155558
$NV = 20$, $NT = 20$	0.437825	1.090947	2.115304	3.179376	4.145775
$NV = 30$, $NT = 30$	0.437921	1.091185	2.115769	3.180081	4.146705
$NV = 40$, $NT = 40$	0.437898	1.091128	2.115658	3.179912	4.146481
ANSYS CFX 12.0	0.438376	1.092310	2.117910	3.183200	4.150640

For a full convergence to five significant digits, more terms (e.g., $NV = 40$ and $NT = 40$) are required. As would be expected, convergence rates of the vertical velocity areslower than those of the temperature, which is due to the fact that the velocity is proportional to the first derivative of the streamfunction (Eq. (6b)), while the temperature is defined by the original eigenfunction expansions (Eq. (30b)). This behavior becomes more apparent as Ra increases, but a full convergence to four significant digits still can be obtained for most cases. The results are in excellent agreement with the ones calculated by ANSYS CFX 12.0, which verifies the accuracy of the GITT solution.

The highest dimensionless temperatures, the corresponding positions and the spatially averaged dimensionless temperatures for a cavity with adiabatic horizontal walls at several values of Ra are summarized in Table 2. The GITT yields good agreement with the solution obtained by ANSYS CFX 12.0, with coincidence of four digits for θ_{max} and three digits for θ_{av}. The peak temperature increases and the average temperature decreases monotonically with Ra; at $Ra = 10000$, the value of θ_{av} is nearly 1.7% lower than that at $Ra = 1000$, which indicates that convection contributes more to heat transport as Ra increases. The variations of θ_{max} and θ_{av} with Ra are plotted in Fig. 3 on a linear-log scale, where the GITT solution curves are constructed by the corresponding values computed for every increment of 200 in Rayleigh numbers.

Table 2: The values of θ_{max} and θ_{av} at different Ra numbers for the cavity with adiabatic horizontal walls, and comparison with the numerical solution by ANSYS CFX 12.0

	$Ra = 1000$	$Ra = 2500$	$Ra = 4900$	$Ra = 7500$	$Ra = 10000$
GITT					
θ_{max}	0.126311	0.128171	0.130814	0.133145	0.134844
x	0.500	0.500	0.500	0.500	0.500
y	1.000	1.000	1.000	1.000	1.000
θ_{av}	0.083316	0.083229	0.082943	0.082461	0.081873
ANSYS CFX 12.0					
θ_{max}	0.126321	0.128189	0.130835	0.133168	0.134867
x	0.500	0.500	0.500	0.500	0.500
y	0.995	1.000	0.995	1.000	1.000
θ_{av}	0.083327	0.083239	0.082952	0.082469	0.081879

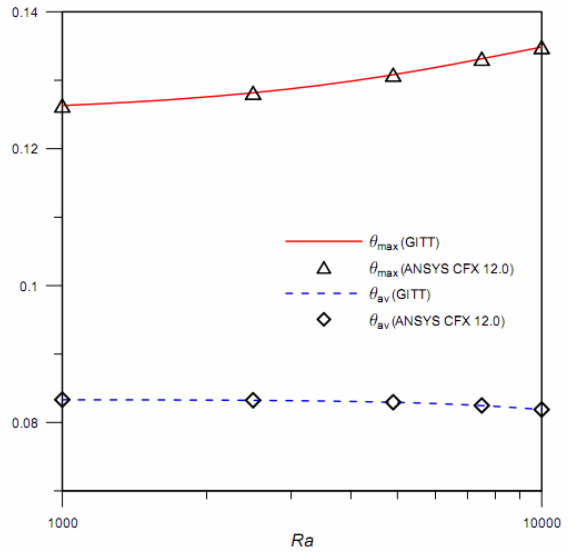

Figure 3: Variations of the maximum dimensionless temperature θ_{max} and spatially averaged dimensionless temperature θ_{av} with Ra for a cavity with adiabatic horizontal walls, and the comparison with the results obtained by ANSYS CFX 12.0.

Figs. 4 and 5 show the variation of the dimensionless temperature θ and the profile of the dimensionless vertical velocity V along the horizontal centerline at $Ra = 4900$, respectively. Fig. 6 reports the profile of the dimensionless horizontal velocity U along $y = 0.75$ at $Ra = 4900$. The results are compared with numerical simulations carried out by ANSYS CFX 12.0, for which a close agreement is observed.

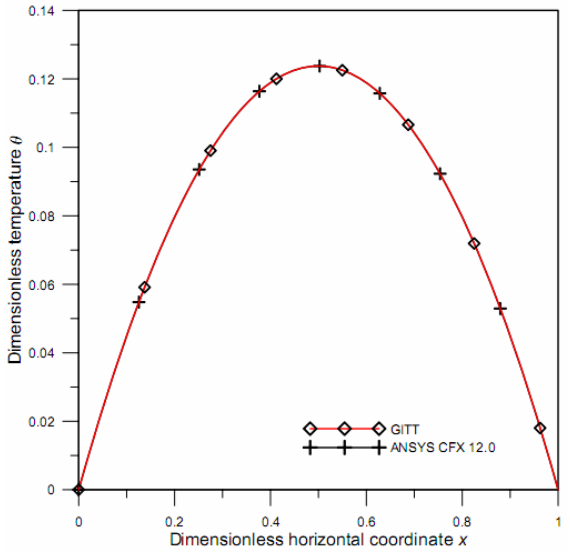

Figure 4: Variation of the dimensionless temperature θ along the horizontal centerline at $Ra = 4900$ for a cavity with adiabatic horizontal walls.

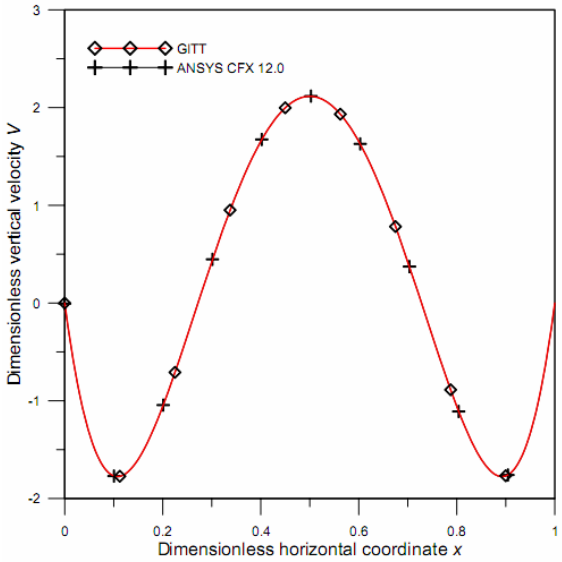

Figure 5: Profile of the dimensionless vertical velocity V along the horizontal centerline at $Ra = 4900$ for a cavity with adiabatic horizontal walls.

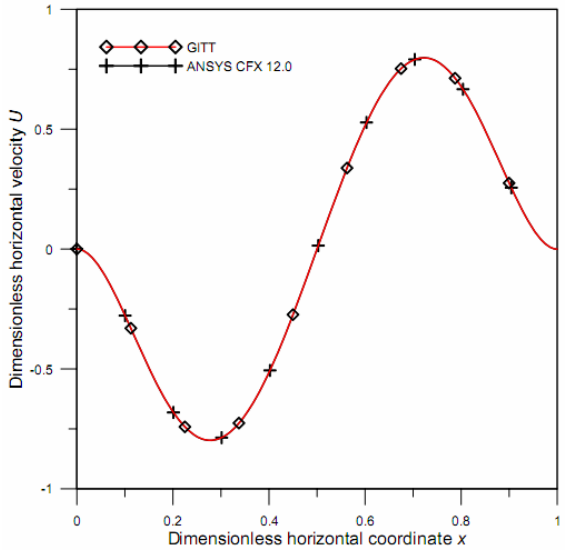

Figure 6: Profile of the dimensionless horizontal velocity U along $y = 0.75$ at $Ra = 4900$ for a cavity with adiabatic horizontal walls.

The steady-state dimensionless stream function ψ and temperature θ for a cavity with isothermal walls at $Ra = 10000$ are shown in Fig. 7. The streamline exhibits flow behavior similar to that obtained for a cavity with adiabatic horizontal walls; only one circulation cell forms in each half of the enclosure, with a perfect bilateral symmetry. It can be noted that the streamfunction values when all walls are isothermal are approximately half of the corresponding values

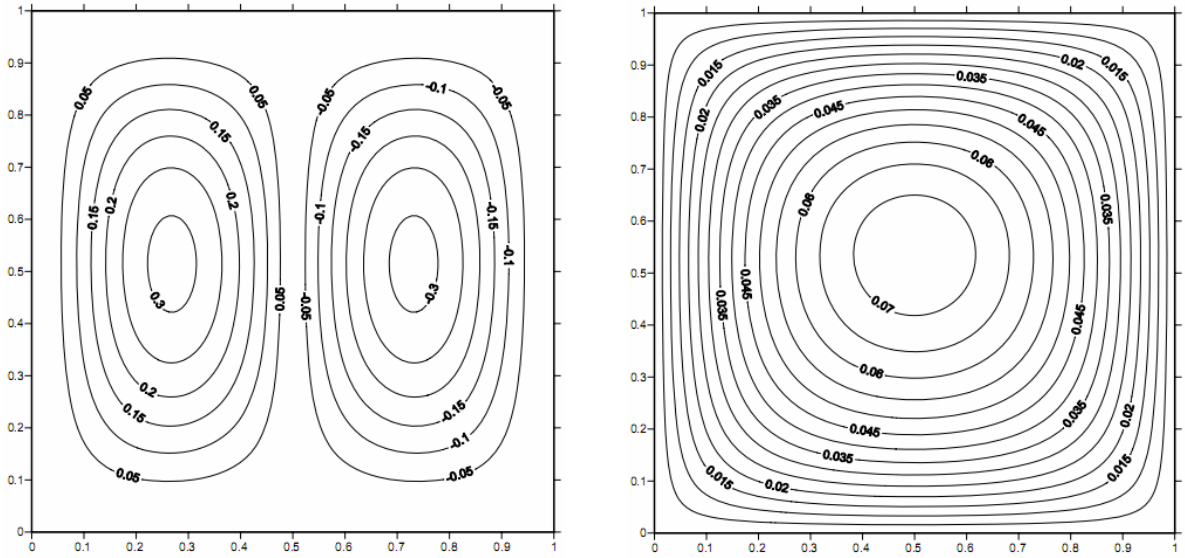

(a) (b)

Figure 7: Contour plots for an internally heated square enclosure with isothermal walls at $Ra = 10000$: (a) streamline, (b) isotherm.

for the case with adiabatic horizontal walls, which has been also captured by Joshi *et al*. (2006). With an approximate up-down symmetry, the isotherm plot indicates that the maximum dimensionless temperature occurs nearly at the center of the cavity and the lowest temperature is located along the side walls.

An analysis similar to the above is performed on the convergence behavior of the dimensionless temperature θ and dimensionless vertical velocity V at the center point of a cavity with isothermal walls, as shown in Table 3. In this case, the Rayleigh numbers are set equal to 1000, 2500, 4900, 7500 and 10000, respectively. For reference purposes, parallel computations are implemented with ANSYS CFX 12.0. The excellent convergence rates of both θ and V give agreement to four significant digits, with values of $NV \le 40$ and $NT \le 40$.

The values of θ_{max} and θ_{av} for a cavity with isothermal walls are listed in Table 4 to corroborate the accuracy of the GITT solution, irrespective of the magnitude of Ra. Compared to the case with adiabatic horizontal walls, a different behavior is found for the maximum temperature, which declines slightly and the corresponding location moves upward continuously as the value of Ra increases. The value of θ_{max} at $Ra = 10000$ is about 0.32% lower than that at $Ra = 1000$.

Table 3: Convergence of the dimensionless temperature θ and dimensionless vertical velocity V with different truncation orders NV and NT for the cavity with isothermal walls, and comparison with the numerical solution by ANSYS CFX 12.0 at center point

	$Ra = 1000$	$Ra = 2500$	$Ra = 4900$	$Ra = 7500$	$Ra = 10000$
$\theta(0.5, 0.5)$					
$NV = 10, NT = 10$	0.073726	0.073694	0.073585	0.073390	0.073133
$NV = 20, NT = 20$	0.073657	0.073625	0.073516	0.073321	0.073064
$NV = 30, NT = 30$	0.073668	0.073635	0.073526	0.073332	0.073074
$NV = 40, NT = 40$	0.073664	0.073632	0.073523	0.073328	0.073071
ANSYS CFX 12.0	0.073676	0.073643	0.073534	0.073339	0.073081
$V(0.5, 0.5)$					
$NV = 10, NT = 10$	0.213858	0.534340	1.045302	1.594469	2.116263
$NV = 20, NT = 20$	0.213155	0.532583	1.041866	1.589227	2.109303
$NV = 30, NT = 30$	0.213223	0.532753	1.042198	1.589734	2.109977
$NV = 40, NT = 40$	0.213206	0.532713	1.042119	1.589613	2.109816
ANSYS CFX 12.0	0.213439	0.533295	1.043250	1.591330	2.112080

Table 4: The values of θ_{max} and θ_{av} at different Ra numbers for the cavity with isothermal walls, and comparison with the numerical solution by ANSYS CFX 12.0

	$Ra = 1000$	$Ra = 2500$	$Ra = 4900$	$Ra = 7500$	$Ra = 10000$
GITT					
θ_{max}	0.073668	0.073655	0.073612	0.073534	0.073432
x	0.500	0.500	0.500	0.500	0.500
y	0.505	0.510	0.520	0.530	0.538
θ_{av}	0.035143	0.035138	0.035121	0.035089	0.035048
ANSYS CFX 12.0					
θ_{max}	0.073681	0.073666	0.073623	0.073546	0.073442
x	0.500	0.500	0.500	0.500	0.500
y	0.505	0.510	0.520	0.530	0.540
θ_{av}	0.035153	0.035148	0.035130	0.035099	0.035058

Figures 8 and 9 depict the variation of the dimensionless temperature θ and the profile of the dimensionless vertical velocity V along the horizontal centerline at $Ra = 7500$ for a cavity with isothermal walls, respectively. Figure 10 reports the profile of the dimensionless horizontal velocity U along $y = 0.75$ at $Ra = 7500$. The plots are qualitatively similar to the ones obtained from a cavity with adiabatic horizontal walls at $Ra = 4900$. It is observed that the direction of the horizontal velocity changes its sign at around $x = 0.5$, while the vertical velocity is positive throughout the central region of the cavity and negative near the boundaries.

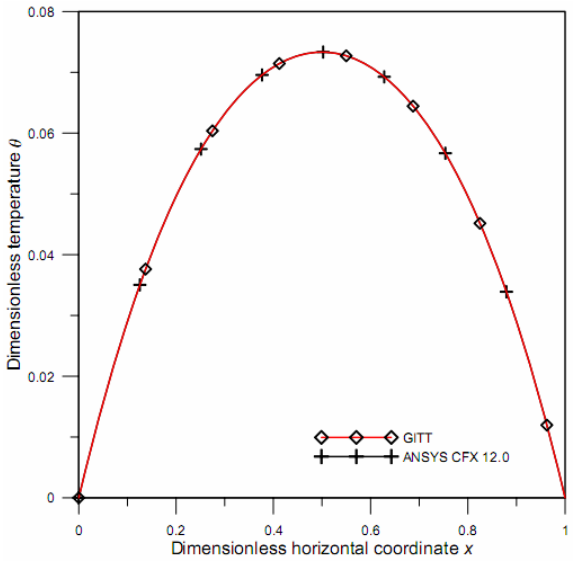

Figure 8: Variation of the dimensionless temperature θ along the horizontal centerline at $Ra = 7500$ for a cavity with isothermal walls.

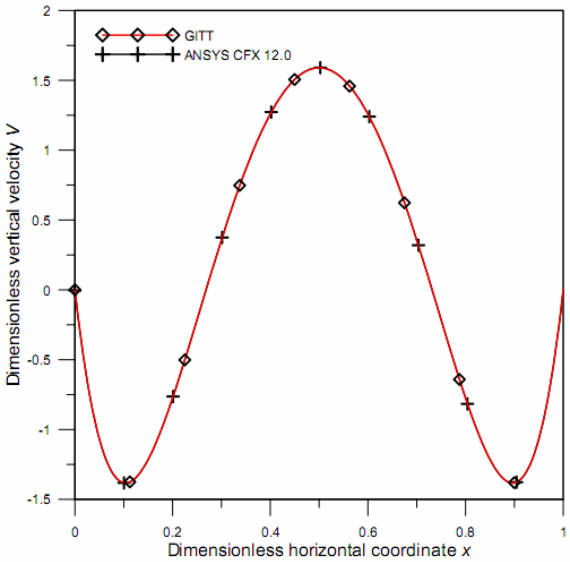

Figure 9: Profile of the dimensionless vertical velocity V along horizontal centerline at $Ra = 7500$ for a cavity with isothermal walls.

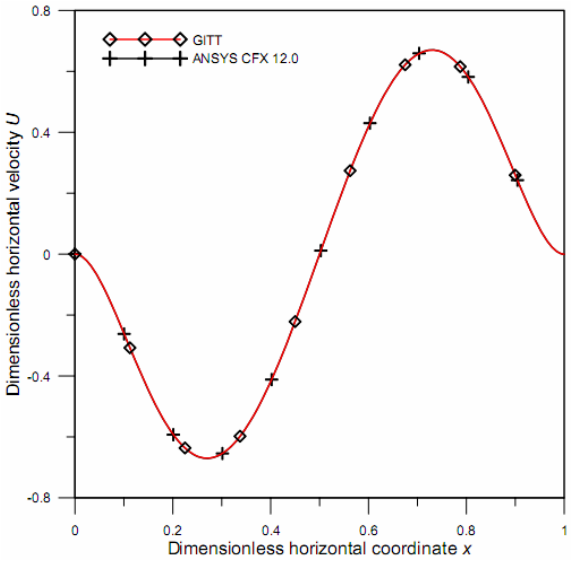

Figure 10: Profile of the dimensionless horizontal velocity U along $y = 0.75$ at $Ra = 7500$ for a cavity with isothermal walls.

CONCLUSIONS

The generalized integral transform technique (GITT) has been shown in this work to be an adequate approach for the analysis of natural convection in a square cavity containing internal energy sources, providing an accurate numerical-analytical solution for the temperature and velocity components. The numerical results reported are in excellent agreement with the solution obtained by ANSYS CFX 12.0, which supports the validity of the present computations. This approach can be either employed for benchmarking purposes, yielding sets of reference orders and exceptional computational performances. It is important to note that the methodology developed is applicable to any boundary conditions, and may also be applied to the analysis of natural convection in a rectangular cavity with different aspect ratios or an inclined cavity.

ACKNOWLEDGMENTS

The authors gratefully acknowledge the financial support provided by CNPq, CAPES and FAPERJ of Brazil for their research work. Chen An also would like to acknowledge the financial support provided by the China Scholarship Council.

NOMENCLATURE

g	acceleration due to gravity	m s^{-2}
H	cavity length and height	m
k	thermal conductivity	W m^{-1} K^{-1}
M_m	normalization integral	
N_i	normalization integral	
NT	truncation order in the temperature expansions	
NV	truncation order in the streamfunction expansions	
p	pressure	Pa
Pr	Prandtl number	
q'''	heat generation per unit volume	W m^{-3}
Ra	Rayleigh number	
T	temperature	K
T_o	temperature at the boundaries	K
u	velocity component in the x-direction	m s^{-1}
U	dimensionless velocity component in the x-direction	
v	velocity component in the y-direction	m s^{-1}
V	dimensionless velocity component in the y-direction	
x	dimensionless space coordinate	
y	dimensionless space coordinate	
X_i	eigenfunction	
$\tilde{X}_i$	normalized eigenfunction	

Greek Letters

α	fluid thermal diffusivity	m^{2}s^{-1}
β	thermal expansion coefficient	K^{-1}
β_m	eigenvalue	
θ	dimensionless temperature	
$\overline{\theta}$	dimensionless transformed temperature	
θ_{av}	spatially averaged dimensionless temperature	
θ_{max}	maximum dimensionless temperature	
ϕ_m	eigenfunction	
$\overline{\phi}_m$	normalized eigenfunction	

ψ	dimensionless streamfunction	
$\bar{\psi}$	transformed streamfunction	
μ_i	eigenvalue	
ν	kinematic viscosity	m^2s^{-1}

Superscript

*	dimensional variables

Subscripts

i,m	eigenquantities orders

REFERENCES

Acharya, S., Goldstein, R. J., Natural-convection in an externally heated vertical or inclined square box containing internal energy-sources. Journal of Heat Transfer-Transactions of the ASME, 107(4), 55-865 (1985).

An, C., Su, J., Dynamic response of clamped axially moving beams: Integral transform solution. Applied Mathematics and Computation, 218(2), 249-259 (2011).

Arcidiacono, S., Ciofalo, M., Low-Prandtl number natural convection in volumetrically heated rectangular enclosures III. Shallow cavity, AR = 0.25. International Journal of Heat and Mass Transfer, 44(16), 3053-3065 (2001).

Arcidiacono, S., Di Piazza, I., Ciofalo, M., Low-Prandtl number natural convection in volumetrically heated rectangular enclosures II. Square cavity, AR = 1. International Journal of Heat and Mass Transfer, 44(3), 537-550 (2001).

Baker, L., Faw, R. E., Kulacki, F. A., Postaccident heat removal - Part I: Heat transfer within an internally heated, nonboiling liquid layer. Nuclear Science and Engineering, 61(2), 222-230 (1976a).

Baker, L., Faw, R. E., Kulacki, F. A., Postaccident heat removal - Part II: Heat transfer from an internally heated liquid to a melting solid. Nuclear Science and Engineering, 61(2), 231-238 (1976b).

Bethe, H. A., Energy production in stars. Science, 161(3841), 541-547 (1968).

Cheng, C. Y., Non-Darcy natural convection heat and mass transfer from a vertical wavy surface in saturated porous media. Applied Mathematics and Computation, 182(2), 1488-1500 (2006).

Cheng, C. Y., Natural convection boundary layer flow of fluid with temperature-dependent viscosity from a horizontal elliptical cylinder with constant surface heat flux. Applied Mathematics and Computation 217(1), 83-91 (2010).

Cotta, R. M., Integral Transforms in Computational Heat and Fluid Flow. CRC Press, Boca Raton, FL (1993).

Cotta, R. M., The Integral Transform Method in Thermal and Fluids Science and Engineering. Begell House, New York (1998).

Cotta, R. M., Mikhailov, M. D., Heat Conduction - Lumped Analysis, Integral Transforms, Symbolic Computation. Ed. John Wiley & Sons, Chichester, England (1997).

Daniels, P. G., Jones, O. K., Convection in a shallow rectangular cavity due to internal heat generation. International Journal of Heat and Mass Transfer, 41(23), 3979-3987 (1998).

Di Piazza, I., Ciofalo, M., Low-Prandtl number natural convection in volumetrically heated rectangular enclosures I. Slender cavity, AR = 4. International Journal of Heat and Mass Transfer, 43(17), 3027-3051 (2000).

Fusegi, T., Hyun, J. M., Kuwahara, K., Numerical study of natural-convection in a differentially heated cavity with internal heat-generation - Effects of the aspect ratio. Journal of Heat Transfer-Transactions of the ASME, 114(3), 773-777 (1992).

IMSL, IMSL Fortran Library version 5.0. MATH/ LIBRARY Volume 2. Visual Numerics, Inc., Houston, TX (2003).

Joshi, M. V., Gaitonde, U. N., Mitra, S. K., Analytical study of natural convection in a cavity with volumetric heat generation. Journal of Heat Transfer-Transactions of the ASME, 128(2), 176-182 (2006).

Kairi, R. R., Murthy, P. V. S. N., Effect of viscous dissipation on natural convection heat and mass transfer from vertical cone in a non-newtonian fluid saturated non-darcy porous medium. Applied Mathematics and Computation, 217(20), 8100-8114 (2011).

Kawara, Z., Kishiguchi, I., Aoki, N., Michiyoshi, I., Natural convection in a vertical fluid layer with internal heating. In: Proceedings of the 27th National Heat Transfer Symposium of Japan. Vol. II. pp. 115-117 (1990).

Leal, M. A., Machado, H. A., Cotta, R. M., Integral transform solutions of transient natural convection in enclosures with variable fluid properties. International Journal of Heat and Mass Transfer, 43(21), 3977-3990 (2000).

Leal, M. A., Pérez-Guerrero, J. S., Cotta, R. M., Natural convection inside two-dimensional cavities: The integral transform method. Communications in Numerical Methods in Engineering, 15, 113-125 (1999).

Lee, J. H., Goldstein, R. J., An experimental-study on natural-convection heat-transfer in an inclined

square enclosure containing internal energy-sources. Journal of Heat Transfer-Transactions of the ASME, 110(2), 345-349 (1988).

May, H. O., A numerical study on natural-convection in an inclined square enclosure containing internal heat-sources. International Journal of Heat and Mass Transfer, 34(4-5), 919-928 (1991).

Mckenzie, D. P., Roberts, J. M., Weiss, N. O., Convection in earth's mantle - Towards a numerical-simulation. Journal of Fluid Mechanics, 62, 465-538 (1974).

Qiu, S. Z., Qian, L. B., Zhang, D. L., Su, G. H., Tian, W. X., Numerical research on natural convection in molten salt reactor with non-uniformly distributed volumetric heat generation. Nuclear Engineering and Design, 240(4), 796-806 (2010).

Rahman, M., Sharif, M. A. R., Numerical study of laminar natural convection in inclined rectangular enclosures of various aspect ratios. Numerical Heat Transfer Part A-Applications 44 (4), 355-373 (2003).

Runcorn, S. K., Convection currents in earth's mantle. Nature, 195(4848), 1248-1249 (1962).

Tritton, D. J., Internally heated convection in atmosphere of venus and in laboratory. Nature, 257(5522), 110-111 (1975).

Wolfram, S., The Mathematica Book. 5th Ed. Wolfram Media/Cambridge University Press, Champaign, IL, USA (2003).